TITLE: Fatigue Crack Growth Predictions for Simplified Spectrum Loading: Influence of Major Cycles on Minor-Cycle Damage Rates

TITLE: Aging Mechanisms and Control. Symposium Part A - Developments in Computational Aero- and Hydro-Acoustics. Symposium Part B - Monitoring and Management of Gas Turbine Fleets for Extended Life and Reduced Costs [Les mecanismes vieillissants et le controle] [Symposium Partie A - Developpements dans le domaine de l'aeroacoustique et I'hydroacoustique numeriques] [Symposium Partie B ...

Fatigue Crack Growth Predictions for Simplified Spectrum Loading: Influence of Major Cycles on Minor-Cycle Damage Rates

Stephan M. Russ,[1] Andrew H. Rosenberger,[1] James M. Larsen,[1] and W. Steven Johnson[2]

[1]U.S. Air Force, Air Force Research Laboratory
Materials and Manufacturing Directorate
AFRL/MLLMN, 2230 Tenth Street, Ste 1
Wright-Patterson Air Force Base, Ohio 45433-7817, U.S.A.

[2]Georgia Institute of Technology
School of Materials Science and Engineering
Atlanta, GA 30332-0245, USA

ABSTRACT

As part of the Engine Structural Integrity Program, USAF turbine-engine components are subject to a damage tolerance or crack-growth assessment. This assessment involves the prediction of crack-growth lifetimes from an initial flaw size under simulated mission loading. The accuracy of the prediction is dependent upon numerous assumptions and inputs: how well the actual mission is simulated by the simpler load spectrum, the accuracy of the component temperature and stress analysis, the ability to account for load-history effects and time dependency using steady-state crack-growth data, and accounting for thermomechanical fatigue crack growth using isothermal data, to name just a few. It is evident that the life prediction is a very complex problem, and numerous effects are accounted for with empirical factors based on experience and laboratory observations. However, understanding the damage mechanisms and their controlling variables is essential in improving the accuracy of crack-growth predictions, given the complex nature of the problem.

Based on reported engine mission spectra, some missions can, in their most simple form, be represented by a major cycle, representing an engine start-up and shut-down, bracketing numerous minor cycles, resulting from in-flight throttle excursions. The major cycle has a stress ratio near zero, and the minor cycles have stress ratios on the order of 0.4 and above. Depending on the number and severity of the minor cycles, the damage, as predicted by available linear damage summation rules, can be dominated by either the minor or major cycle or these may be more evenly partitioned. Thus, there is a need to quantify the effect of tensile underloads, represented by the major cycle, on the minor cycle and vice versa.

Data have been generated on a titanium compressor-disk alloy (Ti-17) utilizing a stress ratio of 0.4 or 0.7 to represent the minor cycles and 0.1 to represent a major cycle. Results indicate that simple linear-damage rules can over predict crack propagation life, depending on the ratio of minor to major cycles. Several tests were performed in the vicinity of the fatigue crack growth threshold to scrutinize the effect. It is shown that the crack-growth predictions can be enhanced by slight modifications of the stress intensity range. A relatively new load-sequence method was evaluated to determine its merits relative to inveterate approaches. The method is based on a measure of the crack propagation resistance of the system.

INTRODUCTION

Fatigue crack growth predictions have been an essential element of the life-management system for turbine engine components since the mid 1980's. The United States Air Force's (USAF) *Retirement for Cause* (RFC) program [1] demonstrated the potential as well as the benefits, from a sustainment-cost perspective, of managing fracture-critical components based on fatigue crack growth behavior and nondestructive inspections. Today, USAF engines are designed and managed under the *Engine Structural Integrity Program* (ENSIP) [2], which mandates both crack-growth and crack-initiation predictions for all key locations on fracture-critical components. A cornerstone of both RFC

Paper presented at the RTO AVT Symposium on "Ageing Mechanisms and Control: Part B – Monitoring and Management of Gas Turbine Fleets for Extended Life and Reduced Costs", held in Manchester, UK, 8-11 October 2001, and published in RTO-MP-079(I).

and ENSIP is the ability to predict fatigue crack growth, and to do so under realistic load-temperature-time spectra.

The bulk of fatigue crack growth (FCG) studies available in the literature have been performed under constant amplitude loading, otherwise known as steady-state conditions. However, the problem of predicting FCG lives becomes incresingly more difficult under *variable amplitude* or *spectrum loading*, when the steady-state assumptions are violated. Under spectrum loading, results can vary significantly with respect to steady-state predictions depending on the significance of load-interaction effects. It has been demonstaratd by Skorupa [3,4] that the effects can vary depending on the application. Models, like those developed by Newman and Fleck [5-8], based on plasticity-induced closure have enabled an interpretation of significant portions of experimental results. "Some observations, however, which cannot be understood in terms of plasticity-induced crack closure, or which are even in contradiction with the crack closure approach, indicate a possible role of other factors. A general conclusion is that conditions under which various phenomena can affect variable amplitude fatigue crack growth and interactions between them are insufficiently recognized."[4] The lack of a fundamental understanding of the FCG process under variable amplitude loading can lead to excessive safety factors in design and/or inordinate testing to characterize the material response to a limitless number of possible load scenarios.

A majority of load-interaction studies in the literature involve the application of periodic overloads and/or overload - compressive underload cycles which for the turbine engine industry are of academic interest but applicability is questionable. For starters, major, fracture-critical components are not subjected to significant overloads or compressive load excursions. A typical load-temperature-time history for a cooled turbine disk was shown by Larsen and Nicholas [9] to contain only mild overloads, and they occur on such a routine basis that it limits any crack retardation effect. In fact, the overloads were found to " . . . account for much of the crack propagation produced by a fatigue spectrum."[9] Similar conclusions were drawn by an AGARD working group established in the early 1980s to develop a loading standard for fighter aircraft engine disk usage. The working group developed TURBISTAN (TURBIne loading STANdard) [10], a test spectrum applicable for titanium alloys operating at or near ambient temperature. From a breakdown of the TURBISTAN load spectrum, it begins to approximate a simple sequence containing a high stress-ratio baseline with periodic underloads at or near zero. The AGARD study provided further evidence that for rotating turbine-engine components the applicable load spectrum consists of high-R minor cycles and periodic major cycles with minimum loads near zero. Overloads were determined to be of less importance than for airframe structures. However, based on experimental results presented by Raizenne [11], effects of underloads should be taken into account. Also, Jany and Renne [12] demonstrated, through comparisons with life prediction models, that the minor cycles contributed to the fatigue crack growth process and, therefore, could not be neglected.

Relative to research involving overloads, a much smaller number of studies have investigated the effect of underloads in the absence of overloads, and the attention of most of these was on compressive underloads. A general conclusion was that compressive load excursions cannot be neglected during crack growth analysis, and that the underloads can produce FCG rate acceleration and/or a reduction in threshold. [13-18] However, there are cases, such as the study by Yang [19], where no significant load interactions were oserved. In general, increased growth rates were attributed to decreases in closure. Of notable interest is that Yu et.al. [14] demonstrated acceleration of high-R FCG rates, yet the closure models do not predict closure under these high-R conditions. Therefore, the observed FCG acceleration cannot be explained based on closure arguments. This suggests that other phenomena have a prominent role under these load scenerios.

Sehitoglu and colleagues [20-22] have performed finite element analyses of closure, deformation, and residual stresses ahead of a crack. Their recommendations include development of crack propagation models that capture the residual stresses, both in the wake and at the crack tip, and determination of S_{II}, an estimate of when the stresses ahead of a crack first become tensile. They warned that under variable amplitude loading, the difference between the opening load, S_{open}, and S_{II} could become significant. Thus, even in the absence of closure; stress ratio, overload, and underload effects would be expected. These recommendations are consistent with the experimental observations

of Yu et.al. [14] as well as the recent work on load-interaction effects on threshold by Moshier et.al. [23] and Lang [24,25].

The goal of this study was to investigate the effect of tensile underload cycles on the high stress-ratio, fatigue crack-growth response of beta-forged Ti-17, and to guide development of an appropriate lifing methodology to account for observed load-interaction effects. To accomplish these objectives a modified description of the crack driving force, ΔK_{eff}, is proposed from which crack growth rates can be determined on a cycle-by-cycle basis. The modified description of ΔK_{eff} is based on a measure of an instantaneous propagation resistance of the material.

TEST PROCEDURE

Material and Specimen Geometry

Ti-17 is the commercial name for Ti-5Al-2Sn-2Zr-4Mo-4Cr (wt%), an alpha-beta titanium alloy designed for applications at temperatures below 427°C. Redden [26] demonstrated the advantages over Ti-6Al-4V in strength, hardenability, fracture toughness, fatigue crack initiation, and crack growth resistance. However, the property improvements come at an expense of a five-percent increase in density. For this study, specimens were machined from a laboratory-scale pancake forging. The starting billet was forged above the beta transus, with a final reduction ratio of 3.5:1, resulting in a "pancake" with a nominal thickness of 77 mm and diameter of 330 mm. The pancake was solution heat treated and aged to produce a Widmanstatten microstructure, Figure 1. The microstructure consisted of approximately 45% acicular alpha (dark phase) and 55% transformed beta (light phase).

Compact tension, C(T), specimens were machined with the notch oriented in the radial direction of the forging. The C(T) specimens had a thickness of 10 mm, which satisfied plane-strain conditions established by ASTM E399-90 [27]. All other specimen dimensions are shown in Figure 2. The specimens were mechanically polished to a one-micron finish, providing a mirror-like surface to facilitate optical crack-length measurements.

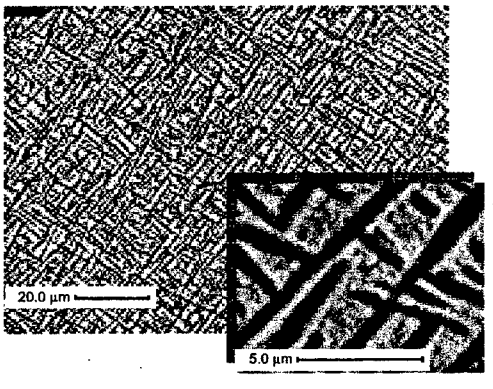

Figure 1. Widmanstatten microstructure of beta-forged Ti-17.

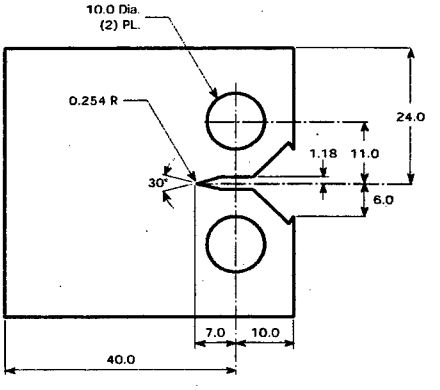

Figure 2. C(T) specimen geometry, dimensions in mm, 10 mm thickness.

Steady-State Fatigue Crack Growth

Baseline, steady-state FCG behavior was evaluated at stress ratios of 0.1, 0.4, and 0.7. All tests were conducted on an MTS servo-hydraulic test frame, and were performed in general accordance with ASTM test specification E647-95a [28]. The C(T) specimens were instrumented with a clip gage at the mouth of the machined notch for measuring crack opening displacements and a direct-current electric potential (DCEP) system for continuous monitoring of crack length. The DCEP technique is described in detail by Hartman and Johnson [29]. A DCEP lead half-spacing of 7 mm was used, and a constant supply current of 2.5 amps was introduced at the top and bottom of the front face of the specimens. Ceramic loading pins and teflon washers were used to electrically isolate the specimen from the load frame. Two traveling microscopes, one on each side of the specimen, were

used to periodically obtain optical, surface, crack-length measurements for comparison to, and post-test correction of, the DCEP measurements. Periodically throughout each test, load-displacement traces were acquired for post-test closure analysis.

Prior to testing, specimens were precracked at a frequency of 5 Hz, R of 0.1, and initial and final K_{max} of 14 and 6 MPa$\sqrt{m}$, respectively, to a final crack length of approximately 10 mm. Actual FCG tests were performed at a frequency of 40 Hz. Fatigue crack growth response was determined from two separate test-control procedures. Immediately following precracking, a K-decreasing test, with a normalized K-gradient of approximately -0.079 mm^{-1}, was performed until crack arrest - defined as less than 0.1 mm crack growth after greater than 5 x 10^6 cycles, i.e. growth rate less than 2 x 10^{-11} m/cycle. This test was followed by a P_{max}-constant test. Fatigue crack growth rates, da/dN, were determined from the crack length versus cycles data utilizing a sliding least squares fit as outlined in ASTM E647-95a, Appendix X1.2 [28].

Propagation Resistance (K_{PR})

Tests similar to those outlined by Lang [24] were performed to determine the propagation resistance, K_{PR}, of the material as a function of stress ratio under constant amplitude conditions. The term propagation resistance refers to an experimentally determined load below which the crack will not propagate, even at stress ranges greater than steady-state threshold. The test set-up was nearly identical to that described for the baseline steady-state FCG tests, with the exception of two modifications to the DCEP system in order to enhance the sensitivity to the onset of crack growth. First, the constant supply current was increased from 2.5 to 9 amps. Second, the DCEP leads were placed just above and below the tip of the machined notch, one on each side of the specimen, as opposed to 7 mm above and below the machined notch along the midline of the front face.

Table 1. Steady-state K_{PR} test matrix and initial results.

PreCrack							
R	$K_{max\ PC}$	a_{PC} (mm)	ΔK	K_{NG}	K_{CG}	K_{PR}	K_{PR} / K_{max}
0.3	13	10.51	2.5	9.42	9.53	7.95	0.61
0.5	18	11.53	2.5	14.03	14.13	12.55	0.70
0.1	10	13.77	2.5	7.42	7.51	5.94	0.59
0.2	11	14.75	2.5	7.98	8.08	6.50	0.59
0.6	20	15.53	2.5	16.64	16.73	15.16	0.76
0.4	15	16.52	2.5	11.43	11.52	9.95	0.66
0.7	22	18.25	2.5	19.08	19.18	17.60	0.80
0.2	12	19.51	2.5	8.59	8.75	7.14	0.60
0.8	25	22	2.36	22.34	22.41	20.85	0.83

All stress intensities (K) have the units MPa$\sqrt{m}$

To characterize K_{PR} after steady-state FCG as a function of R, a series of tests was conducted as shown in Table 1. The sequence of R was randomly selected, with the exception of R equal 0.7 and 0.8. Due to maximum load restrictions of the ceramic pins, these latter two tests had to occur when the crack was longer, when lower applied loads could achieve the desired K_{max} values. For a given R the crack was first grown under constant K_{max} for a minimum of 0.5 mm to ensure that steady-state crack growth conditions were achieved. Following the precrack, K_{PR} was measured using the load-step technique depicted schematically in Figure 3. A series of load blocks was applied with each successive block being stepped by nominally 0.1 MPa$\sqrt{m}$. Each block consisted of 400,000 cycles at 40 Hz, and ΔK was held constant at 2.5 MPa$\sqrt{m}$. Note that the ΔK of the blocks was decreased for the R of 0.8 condition in order to keep the minimum load of the first block from being less than the precrack minimum load. The load steps continued until the crack began to grow, resolved by an increase in the DCEP voltage. A "snapshot" of the test - consisting of the load, DCEP voltage, and temperature - was recorded once every 20 seconds. An example is shown in Figure 4, where the DCEP voltage is overlaid on the recorded loads. Precracking and the onset of crack growth during block 11 are apparent, characterized by a positive slope of the DCEP voltage. Post test analysis was performed to determine K_{CG} and K_{NG}, the stress intensities of the load blocks when the crack began to grow and the last one where the crack did not grow, respectively. K_{PR} was then

calculated using Equation 1, where ΔK_T equal to 1.53 MPa$\sqrt{m}$ was used as the intrinsic threshold for this material.

$$K_{PR} = \frac{(K_{NG} + K_{CG})}{2} - \Delta K_T \quad (1)$$

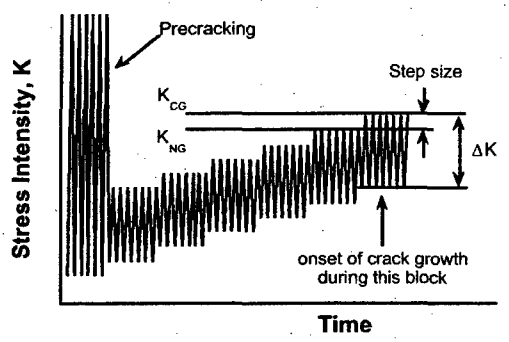

Figure 3. Schematic of loading sequence for measurement of K_{PR}.

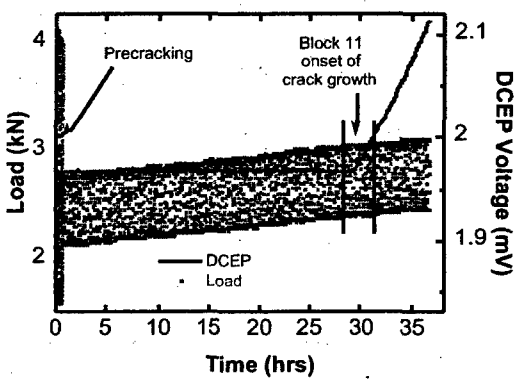

Figure 4. DCEP voltage and load versus time for determination of K_{PR} for precrack conditions K_{max} = 15 MPa$\sqrt{m}$ and R = 0.4.

Simple-Sequence Load-Interaction Tests

To investigate load-interaction effects, a simple sequence spectrum (SSS) was created consisting of a number of high-R baseline cycles with periodic tensile underloads. The high-R baseline ($R_{BL} = P_{min,BL}/P_{max}$) was applied at R of either 0.7 or 0.4, and the underload consisted of an R of 0.1 cycle ($R_{UL} = P_{min,UL}/P_{max}$). A schematic is shown in Figure 5. The number of baseline cycles, N_{BL}, was varied from 10 to 100 to 1000 to examine acceleration / deceleration of the FCG response relative to the baseline cycles. As suggested previously, due to the relative growth rates of the high and low R cycles, it would be difficult, if not impossible, to discern any change in FCG rates without ensuring the baseline cycles contribute a significant percentage of the crack growth. The test matrix executed is presented in Table 2.

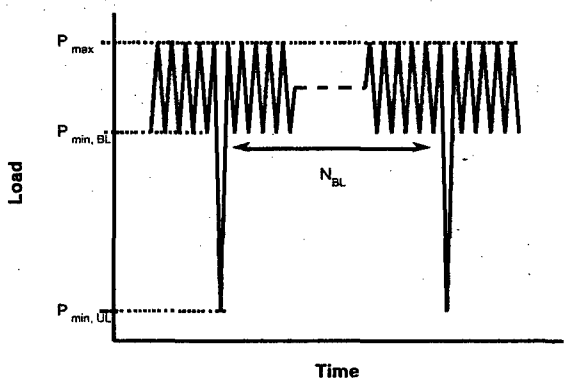

Figure 5. Schematic of simple sequence spectrum (SSS).

For the eight simple-sequence tests the specimen set-up was identical to that used for the steady-state FCG tests described previously. Prior to application of the spectrum loading, specimens were precracked at R of 0.1 and a frequency of 5 Hz under K-decreasing conditions. A minimum of 0.33 mm of crack extension was produced during precracking to ensure the crack was removed from history effects from any previous tests on the same specimen. The final load during precrack was

approximately equal to the maximum load of the subsequent simple-sequence test. Tests were performed under P_{max}-constant conditions at a frequency of 15 Hz, and P_{max} was selected to establish the initial ΔK of the baseline cycles at or near ΔK_{th}. The applied load, initial conditions, the number of blocks (i.e. the times the load sequence was applied), and final conditions are provided in Table 2. Test nomenclature is provided in the left-hand column to facilitate later reference to specific tests.

Table 2. Simple-sequence spectrum (SSS) test matrix and initial results.

Test Nomenclature	Spectrum Definition				Initial		Blocks	Final	
	R_{BL}	N_{BL}	R_{UL}	Load (kN)	a_i (mm)	$K_{max,i}$ (MPa√m)		a_f (mm)	$K_{max,f}$ (MPa√m)
SSS07-10	0.7	10	0.1	2.82	10.39	7.17	349,050	17.29	11.24
SSS07-10	0.7	10	0.1	1.46	20.02	7.06	264,450	23.98	9.95
SSS07-100	0.7	100	0.1	2.00	15.71	7.15	65,390	19.49	9.30
SSS07-1000	0.7	1000	0.1	2.85	10.21	7.14	9,500	14.00	9.13
SSS04-10	0.4	10	0.1	1.15	18.41	4.95	323,860	25.31	9.00
SSS04-10	0.4	10	0.1	0.61	24.32	4.30	488,090	27.52	6.17
SSS04-100	0.4	100	0.1	1.47	11.78	4.44	54,940	15.05	5.48
SSS04-1000	0.4	1000	0.1	1.26	14.66	4.21	15,050	17.81	5.20

RESULTS / DISCUSSION

A straightforward technique, the linear-damage summation model, was concluded to be adequate in predicting simple-sequence tests in both the AGARD study [12] and the work by Yang [19] without including interaction effects. The latter study was based on a comparison of FCG rates, and the former was based on cycles to grow a crack a prescribed amount. The AGARD results are of especial interest, since this study also represents the foremost FCG study published on Ti-17.

Steady-State Fatigue Crack Growth

A hyperbolic arctangent model, Equation 2, was used to fit the experimental growth rate data.

$$\log\left(\frac{da}{dN}\right) = C_1 \arctan h\left\{C_2\left[\log(\Delta K) + C_3\right]\right\} + C_4 \qquad (2)$$

where ΔK is the applied stress intensity range, $\frac{da}{dN}$ is the FCG rate, and C_1 through C_4 are constants manipulated to best represent the data. In the curve-fitting practice, the near-threshold data were weighted to give as good a fit as possible to the very low crack growth regime - since life predictions for gas turbine engines are most sensitive to this portion of the FCG curve.

The experimental FCG rate data and hyperbolic arctangent fits for all three stress ratios are shown in Figure 6. There is very good agreement between the K-decreasing and P_{max}-constant portions of the data sets. The fits from Equation 2 represent the data very well, especially in the difficult-to-fit near-threshold regime which is a strength of the hyperbolic arctangent model. [30] Figure 6 also displays the expected stress ratio dependence. The data layer as a function of R; as R increases, growth rates increase (for the same applied ΔK) and ΔK_{th} decreases.

A common methodology to collapse FCG rate curves as a function of stress ratio is to plot the rates versus ΔK_{eff} instead of $\Delta K_{applied}$, where $\Delta K_{eff} = K_{max} - K_{op}$, and K_{op} is the stress intensity when the crack opens during the loading cycle. Figure 7 shows representative load-displacement traces as the crack extends for the R of 0.1 test. The loads have been normalized with respect to P_{max}, and displacements have been adjusted based on the range and sequentually incremented for ease of presentation. The load-displacement traces exhibited an extended linear upper range, and a line was fit through this upper portion to facilitate closure analysis. For this test closure was negligible immediately following precracking and increased continuously to a level of approximately 0.25 as indicated in the figure. Similar load-displacement traces for the R of 0.4 and 0.7 tests were completely linear, therefore, no closure was detected, and attempts to collapse the FCG curves using closure analysis of this type would be fruitless.

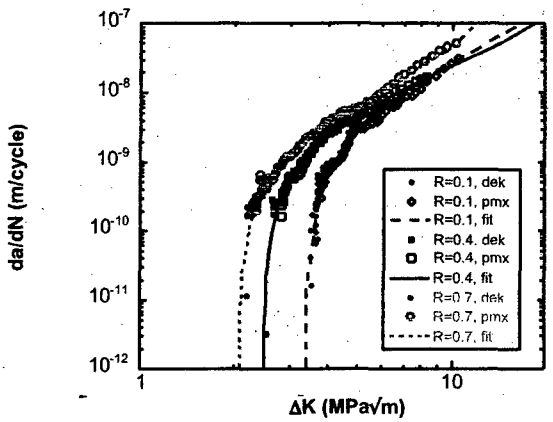

Figure 6. Steady-state, FCG rate data and hyperbolic arctangent fits. Note that in the legend *dek* refers to K-decreasing and *pmx* refers to P_{max}-constant test data.

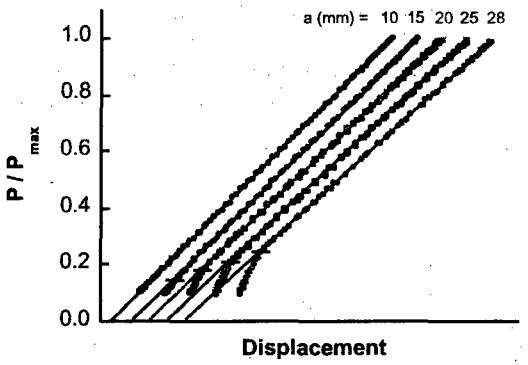

Figure 7. Representative load-displacement traces for R = 0.1 FCG test.

Propagation Resistance (K_{PR})

The results from the tests outlined in Table 1, K_{PR} normalized with respect to K_{max} of the precrack as a function of R during precracking, are graphically shown in Figure 8. A polynomial fit to the data is also displayed based on Equation 3,

$$\frac{K_{PR}}{K_{\max,pc}} = A_1 + A_2 R + A_3 R^2 \tag{3}$$

where A_1, A_2, and A_3 are constants having values of 0.572, 0.066, and 0.361, respectively, and adequately represented the data. It is envisioned that K_{PR}, calculated from Equation 3, can be used in establishing a ΔK_{eff} which sufficiently accounts for stress-ratio dependence of steady-state FCG behavior and ultimately can be used in load-interaction FCG algorithms. For the case of modeling load-interactions, the attraction of using K_{PR}, and ΔK_{eff} as defined by Equation 4, is that ΔK_{eff} is less than $\Delta K_{applied}$ even at R greater than 0.7.

$$\Delta K_{eff} = K_{\max} - K_{PR} \tag{4}$$

However, prior to suggesting K_{PR} be used to model load-interaction effects, it must be demonstrated that it can collapse the stress-ratio dependence of FCG behavior. In other words, there should be a characteristic curve of growth rate described by ΔK_{eff}. To demonstrate, the steady-state data were used along with K_{PR} calculated using Equation 3. A hyperbolic arctangent fit, Equation 5, was fit to all three data sets, R of 0.1, 0.4, and 0.7. Equation 5 is similar to Equation 2 with ΔK_{eff} substituted for ΔK.

$$\log\left(\frac{da}{dN}\right) = C_1 \arctan h\left\{C_2\left[\log\left(\Delta K_{eff}\right) + C_3\right]\right\} + C_4 \tag{5}$$

The results are shown in Figure 9. The three data sets collapsed to one curve described effectively by Equation 5 with C_1 of 1.28, C_2 of 1.94, C_3 of –0.70, and C_4 of –7.61. The constants in Equations 3 and 5, along with ΔK_T of 1.53 MPa√m used in Equation 1, were arrived at through an iterative process to minimize the variance between the hyperbolic arctangent fit and the steady-state FCG data.

Simple-Sequence Load-Interaction Tests

Figures 10 and 11 present growth rates as a function of K_{max} for the SSS07 (R_{BL} = 0.7) and SSS04 (R_{BL} = 0.4) series of tests, respectively. K_{max} was selected as the abscissa, because for a given spectrum there is no unique ΔK. Growth rates, da/dB, are displayed in meters per block of cycles.

Repeatability was demonstrated by the proximity of the two tests with 10 baseline cycles. The growth rates contained a larger amount of scatter than the steady-state tests due to an unexplained increase in the noise of the DCEP signal. Notable was that the growth rates did not increase by a simple factor of 10 as the number of baseline cycles increased from 10 to 100 to 1000. This can be attributed to the relative contribution between the baseline and underload cycles to the overall growth.

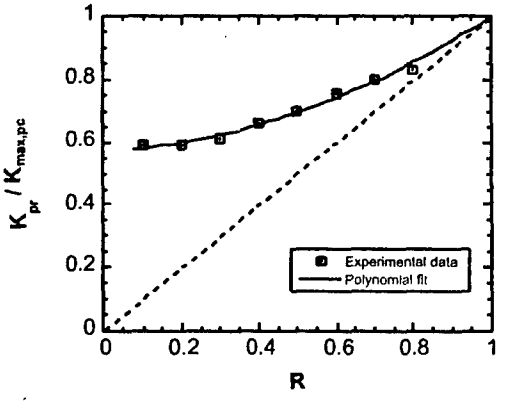

Figure 8. K_{PR} normalized with respect to the precrack K_{max} a function of R during precracking under steady-state conditions.

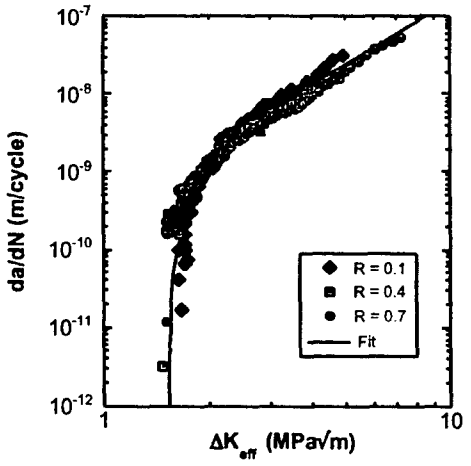

Figure 9. Stress ratio dependence of steady-state FCG behavior described by $\Delta K_{eff} = K_{max} - K_{PR}$.

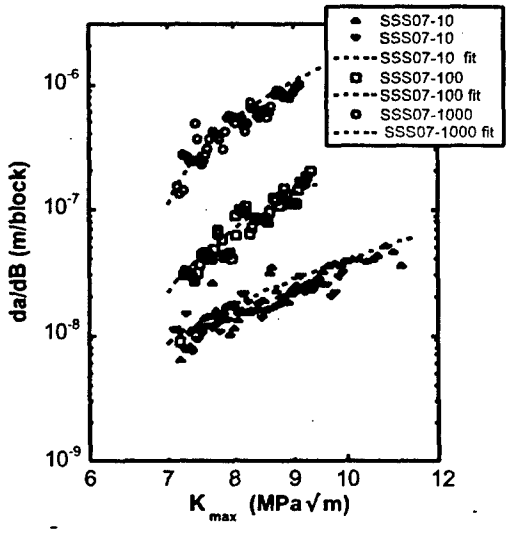

Figure 10. Comparison of predicted and actual FCG rates for SSS07 simple sequence tests.

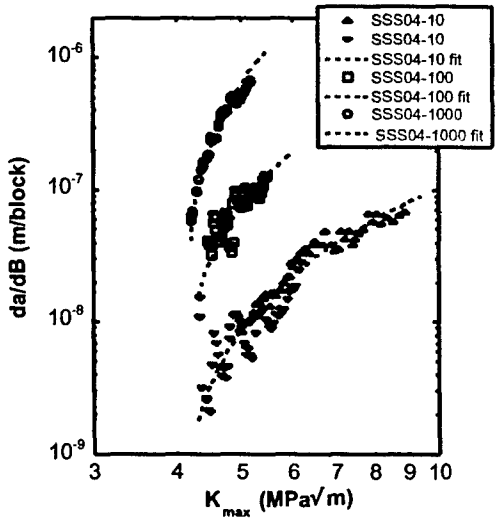

Figure 11. Comparison of predicted and actual FCG rates for SSS04 simple sequence tests.

Linear-Damage Summation Model Without Load-Interaction Effects

Based on success claimed under the AGARD study [12] and Yang [19] in predicting the FCG response for simple-sequence spectra, the linear-damage summation model, ignoring any potential load-interaction effects, was employed to predict the crack growth response from the SSS tests. Linear-damage summation models are simply a summation of predicted crack extension for individual cycles within a block. For the SSS spectra, Equation 6 represented the crack growth for a given block of cycles,

$$\left(\frac{da}{dN}\right)_{Block} = N_{BL}\left(\frac{da}{dN}\right)_{BL} + \left(\frac{da}{dN}\right)_{UL} \quad (6)$$

where N_{BL} is the number of baseline cycles per block, and $\left(\frac{da}{dN}\right)_{BL}$ and $\left(\frac{da}{dN}\right)_{UL}$ are the growth rate per cycle for baseline and underload cycles, respectively. When assuming no load-interaction effects, the steady-state FCG curves were used to represent the growth rates under variable amplitude loading. Thus, $\left(\frac{da}{dN}\right)_{BL}$ and $\left(\frac{da}{dN}\right)_{UL}$ were calculated using the hyperbolic arctangent fits to the steady-state FCG data and the applied ΔK, Equation 2 and Figure 6.

For the tests with R_{BL} of 0.7, the predictions of the no-interaction, linear-damage summation model are presented in column 5 of Table 3. The table displays the results in the form of the ratio of the predicted number of cycles with respect to the experimental, N_{pred} / N_{exp}. Also included is the percent of crack extension attributed to the baseline cycles. For the SSS07-10 tests the predictions were amazingly accurate, within five percent. Noteworthy is that the percent of crack extension attributed to the baseline cycles was less than 30 percent. Therefore, the majority of damage was predicted to be a consequence of the less frequent underload cycles. Hence, if an interaction was occurring, and the baseline cycles were more damaging than assumed, it would not necessarily be apparent within the scatter of FCG data. This is perhaps why both the AGARD study and Yang concluded no interaction was present. As N_{BL} increased from 10 to 100 to 1000, the predictions became increasingly worse. This was interpreted as a true indication that a load-interaction effect was present. Since the underload cycles have a less dominant role as the number of baseline cycles increased, the effect must be manifested as an acceleration of the growth rate of the baseline cycles. As mentioned earlier, other researchers have attributed acceleration of growth rates due to underloads to reductions in closure, and the corresponding increase in ΔK_{eff}. However, in the absence of closure, ΔK_{eff} equals $\Delta K_{applied}$, and ΔK_{eff} can not be increased in this manner. Therefore, a different methodology needs to be devised to allow an increase in the effective crack-growth driving force in the absence of closure.

Table 3. Linear-damage summation model predictions for simple sequence spectrum FCG tests both with and without a load interaction effect.

Test Nomenclature	Spectrum Definition			NO Interaction		With interaction			
	R_{BL}	N_{BL}	Load (kN)	N_{pred} / N_{exp}	% from BL	N_{pred} / N_{exp}	% from BL	BLMF	ULMF
SSS07-10	0.7	**10**	2.82	1.04	29.6	**0.99**	65.8	1.17	0.90
SSS07-10	0.7	**10**	1.46	1.01	23.9	**0.99**	62.4	1.17	0.90
SSS07-100	0.7	**100**	2.00	1.67	70.7	**1.00**	90.9	1.09	0.90
SSS07-1000	0.7	**1000**	2.85	1.93	95.4	**1.00**	98.7	1.06	0.90
SSS04-10	0.4	**10**	1.15	1.16	80.3	**1.01**	86.4	1.045	0.94
SSS04-10	0.4	**10**	0.61	1.38	77.5	**0.98**	89.2	1.045	0.94
SSS04-100	0.4	**100**	1.47	1.47	97.2	**1.01**	98.8	1.040	0.94
SSS04-1000	0.4	**1000**	1.26	1.45	99.6	**0.99**	99.9	1.015	0.94

For the tests with R_{BL} of 0.4, the predictions of the no-interaction, linear-damage summation model are also found in column 5 of Table 3. A load-interaction effect was not as obvious for this series of tests. This was attributed to the less severe underload relative to the minimum load of the baseline cycle. Noteworthy was that the predictions for the SSS04-10 tests were not as accurate as the SSS07-10 tests. For the SSS04-10, in the absence of any load-interaction effect, the percent of crack growth attributed to the baseline cycles was approximately 80 percent, versus less than 30 percent for the SSS07-10 tests. Intuitively, an R of 0.4 cycle is more damaging than an R of 0.7 cycle relative to an R of 0.1 cycle with the same K_{max}. Therefore, if load-interaction effects were occurring, since the R of 0.4 cycles are expected to contribute a significant percentage of the overall crack extension, the effect may be detectable even at a 10-to-1 ratio of baseline-to-underload cycles. The less accurate predictions of the SSS04-10 may then in fact be an indication of the presence of a load-interaction effect. The prediction of the SSS04-100 was worse still. However, when N_{BL} increased to 1000

(SSS04-1000) the prediction relative to the experimental results had about the same accuracy as the SSS04-100. It has been observed by Fleck [31] that interactions, in the form of crack growth rate accelerations, reach a maximum and decay for both very high and very low values of N_{BL}. This suggests that the maximum deviation from a prediction not including interaction effects could be somewhere between N_{BL} of 100 and 1000 for the spectra with R_{BL} of 0.4.

Linear-Damage Summation Model With Load-Interaction Effects Included

As pointed out previously, including an interaction effect using closure techniques is not possible for the SSS07 and SSS04 spectra, since closure was not present at the high-R load conditions. What is needed to better estimate FCG lives under these conditions is a methodology to increase the effective driving force even in the absence of closure. Lang[24] proposed the modified definition of ΔK_{eff} of Equation 4. He attributed K_{PR} to compressive residual stresses ahead of the crack tip, although not necessarily quantifiably. Sehitoglu and colleagues [20-22] have attempted to calculate residual stresses in the process zone ahead of a crack tip, and even suggested they likely play a significant role in controlling the fatigue crack growth process. It would not be difficult to envision K_{PR}, if truly governed by residual stresses ahead of the crack tip, as being affected by load excursions, and Lang [24] has observed such phenomemon.

Based on the success demonstrated utilizing K_{PR} to collapse the stress-ratio dependence of FCG rates, and the attraction that K_{PR} defines a ΔK_{eff} smaller than $\Delta K_{applied}$, even in the absence of closure, it is proposed to utilize K_{PR} to model the load-interaction effects suspected in the SSS tests. Application of this approach acknowledges that for high-R cycles the stresses in the process zone ahead of the crack tip influence the propagation resistance of the material, as characterized by K_{PR}. It is assumed that the occurrence of an underload disturbs the steady-state conditions, lowering the propagation resistance, and allowing accelerated crack growth rates until the steady-state conditions are reestablished.

To accomplish this, K_{PR} must be defined as a transient variable affected by non steady-state conditions. A schematic of how a "transient" K_{PR} could fluctuate from measured steady-state values is depicted in Figure 12. In this figure K_{PR} is initially shown to be equal the steady-state, R of 0.7 condition, as determined from Equation 3 and Figure 8. As a result of the underload, K_{PR} drops below the high-R steady-state value, and the cycles immediately following the underload are more damaging, i.e. larger ΔK_{eff} and higher growth rate. After some number of cycles the steady-state value is again achieved, and the FCG rate equals the steady state. It is also depicted that the R_{UL} of 0.1 underload cycle would be slightly less damaging than predicted from steady-state behavior. A prediction of the crack growth due to the simple-sequence spectra would be accomplished with the following set of equations:

$$\left(\frac{da}{dN}\right)_{Block} = \sum_{n}\left(\frac{da}{dN}\right) \tag{7}$$

$$\log\left(\frac{da}{dN}\right) = C_1 \operatorname{arctanh}\left\{C_2\left[\log\left(\Delta K_{eff}\right) + C_3\right]\right\} + C_4 \tag{8}$$

$$\Delta K_{eff} = K_{\max} - K_{PR(n)} \tag{9}$$

where Equation 7 is the crack growth for a block of n cycles, and the growth increment for each individual cycle within the block would be determined from Equations 8 and 9. The constants for Equation 8 would be those provided from the steady-state data of Figure 9, and $K_{PR(n)}$ would represent the "transient" K_{PR} depicted in Figure 12. Also, ΔK_{eff} would be set equal $\Delta K_{applied}$, in the event $K_{PR(n)}$ was less than K_{min}. What is required is a representation of K_{PR} as a function of the cycle count, n, within a given block.

To evaluate the merit of this approach, the sensitivity of the linear-damage summation model to slight adjustments of ΔK was assessed. Using the hyperbolic arctangent fits to the steady-state data, shown in Figure 6, a ΔK_{eff} was utilized based on multiplication factors applied to the baseline and underload cycles, *BLMF* and *ULMF*, respectively. The linear-damage summation model,

Equation 6, was used with the growth rates and effective stress-intensity factor ranges determined from Equations 10 through 13.

$$\log\left(\frac{da}{dN}\right)_{BL} = C_1 \operatorname{arctanh}\left\{C_2\left[\log\left(\Delta K_{eff,BL}\right) + C_3\right]\right\} + C_4 \tag{10}$$

$$\Delta K_{eff,BL} = BLMF(1 - R_{BL})K_{\max} \tag{11}$$

$$\log\left(\frac{da}{dN}\right)_{UL} = C_1 \operatorname{arctanh}\left\{C_2\left[\log\left(\Delta K_{eff,UL}\right) + C_3\right]\right\} + C_4 \tag{12}$$

$$\Delta K_{eff,UL} = ULMF(1 - R_{UL})K_{\max} \tag{13}$$

Using the multiplication factors, ΔK_{eff} can be adjusted to evaluate the effect of a transient K_{PR}. A schematic is shown in Figure 13 depicting the effect of setting the BLMF equal to 1.17 for N_{BL} of 10 and 1.09 for N_{BL} of 100, given R_{BL} of 0.7, and $K_{PR,steady\text{-}state}$ equal 0.795. It was acknowledged a priori that the following constraints and/or conditions would have to be met if this sensitivity analysis were to demonstrate capability likely described by the approach utilizing $K_{PR(n)}$.

1. For the predictions of the SSS07 tests, *BLMF* must be less than 1.46. Otherwise ΔK_{eff} would be predicted greater than $\Delta K_{applied}$.
2. For the predictions of the SSS04 tests, *BLMF* must be less than 1.215. Otherwise it would be equivalent to K_{PR} for the baseline cycle dropping below the steady-state K_{PR} for R of 0.1.
3. *ULMF* must be less than or equal to one. This assumes that the underload cycle should be less damaging than the R of 0.1 steady-state condition.
4. *ULMF* was maintained constant for a given R_{BL} (not a function of N_{BL}).
5. For the same R_{BL}, *BLMF* should decrease with increasing N_{BL}. This indicates that K_{PR} would move toward the steady-state value with additional fatigue cycles.
6. The *ULMF* for SSS07 series should be less than *ULMF* for SSS04 series. This assumes that the further away from the steady-state value the longer it should take to achieve it.

Of this list, first four were constraints on the sensitivity analysis, and last two were consequences that needed to be demonstrated.

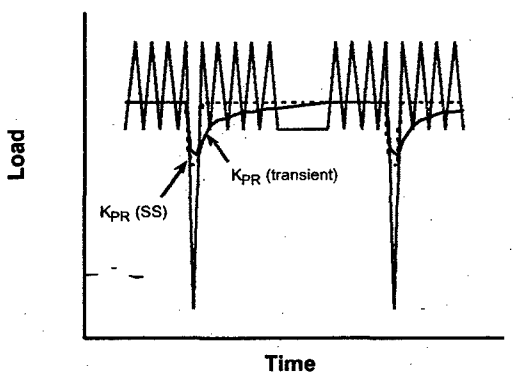

Figure 12. Schematic of a transient K_{PR} to be used in modeling load-interaction effects.

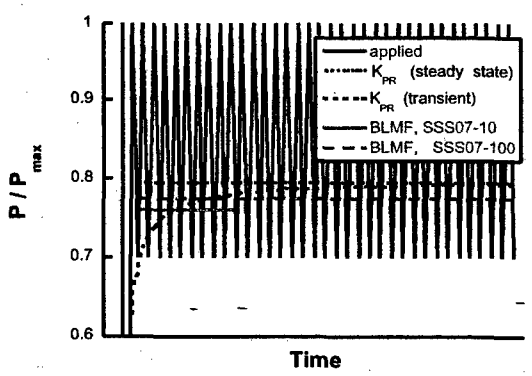

Figure 13. Schematic of how BLMF can simulate the effect of a dynamic K_{PR}.

Values of *BLMF* and *ULMF* were adjusted to best simulate the experimental crack growth data from the simple-sequence spectra. First, the data from the two SSS07-10 tests were used, and a minimization routine was used to best fit the final crack lengths. Both tests could be predicted within one percent by setting *BLMF* to 1.17 and *ULMF* to 0.90. Next the SSS07-100 test was best emulated by decreasing *BLMF* to 1.09 while maintaining *ULMF* at 0.90. Finally, the SSS07-1000 test was emulated while again holding *ULMF* equal 0.90 and decreasing *BLMF* to 1.06. A similar exercise

was accomplished in modeling a load-interaction of the SSS04 series of tests. To best represent these tests lower *BLMFs* and a higher *ULMF* were required. The predictions of the SSS07 and SSS04 series of tests are compared to the experimental data in column 7 of Table 3. Figures 14 and 15 present graphically the predictions with and without the load-interaction incorporated for the SSS07-100 and SSS04-100 tests, respectively. The "fits" of the FCG rates shown in Figures 10 and 11 represent Equation 7 assuming the load interaction effect described. The FCG rates from the model closely resemble the experimental results for all cases tested.

In modeling the test results using this methodology all the constraints previously listed were maintained, and the expected trends observed: *BLMF* decreased with increasing N_{BL}, and *ULMF* was lower for the SSS07 series versus the SSS04 series. The model was made to mimic the data, and does so within two percent of the total blocks to grow the cracks the prescribed amounts. In order to better simulate the crack growth, the percent of crack extension due to the baseline cycles increased significantly, with a corresponding decrease in the relative damage of the underload cycles. This implied that there indeed was a load-interaction effect, and that it manifested itself as an acceleration of the high-R baseline cycles and deceleration of the R of 0.1 underload cycle, relative to steady-state.

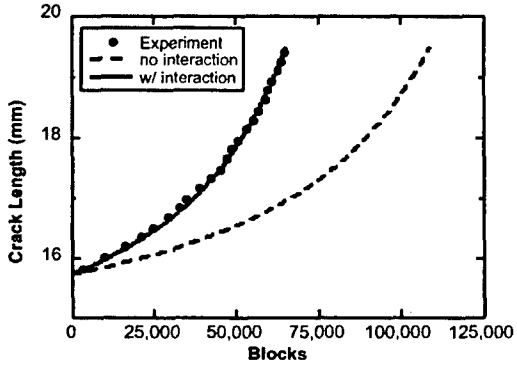

Figure 14. SSS07-100 (R_{BL} = 0.7, N_{BL} = 100) crack growth data compared with predictive models.

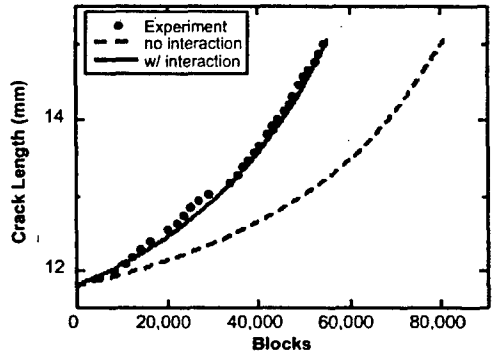

Figure 15. SSS04-100 (R_{BL} = 0.4, N_{BL} = 100) crack growth data compared with predictive models.

CONCLUSIONS

It was demonstrated that underloads, even in tension, can accelerate the crack growth process of high-R baseline cycles for Ti-17. This load-interaction effect was not immediately discernable until the high-R baseline cycles provided the bulk of the crack extension. The data also supported other researcher's observations that load-interactions reach a maximum at an intermittent number of baseline cylces and decay for both high and low values of N_{BL}.

A load-interaction model was proposed that involved the application of a propagation resistance, K_{PR}, in the definition of the effective driving force, ΔK_{eff}, for crack propagation. The merit of the approach was assessed through a simple modification to a linear-damage summation model, which simulated anticipated phenomena. The output from the model incorporating a simple load-interaction effect was made to mimic experimental data of several simple-spectrum tests. In doing so, all a priori constraints were maintained, and anticipated relationships were observed. Thus, it substantiated the hypothesis that a load-interaction effect occurred, and that it was manifested as an acceleration of the high-R baseline cycles and deceleration of the R of 0.1 underload cycle.

K_{PR} is suspected of being a function of the load history and, for high stress ratios, controlled by the stress state ahead of the crack tip. K_{PR} was characterized as a function of stress ratio under steady-state FCG, and successfully demonstrated the capability to collapse the stress-ratio dependence of fatigue crack growth rates. It was hypothesized that the occurrence of an underload disturbs the steady-state conditions ahead of the crack tip, thus, reducing the propagation resistance of the system and accelerating the FCG rate of high-R baseline cycles.

ACKNOWLEDGEMENTS

The authors would like to acknowledge Mr. Ken Goecke for his contributions in experimental test set-up and Mr. Jacob Lawson for his assistance in data analysis.

REFERENCES

1 Harris, J. A., *Engine Component Retirement For Cause, Volume I – Executive Summary*, AFWAL-TR-87-4069, Volume I, AFWAL, Wright-Patterson AFB, OH, 1987.
2 Engine Structural Integrity Program (ENSIP), MIL-STD-1783 (USAF), 30 November 1984.
3 Skorupa, M., *Fatigue and Fracture of Eng Matls and Str*, Vol. 21, No. 8, 1998, pp. 987-1006.
4 Skorupa, M., *Fatigue and Fracture of Eng Matls and Str*, Vol. 22, No. 10, 1999, pp. 905-926.
5 Newman, J. C., Jr., *Methods and Models for Predicting Fatigue Crack Growth under Random Loading, ASTM STP 748*, ASTM, Philadelphia, PA, 1981, pp. 53-84.
6 Newman, J. C., Jr., *Design of Fatigue and Fracture Resistant Structures, ASTM STP 761*, American Society for Testing and Materials, Philadelphia, PA, 1982, pp. 255-277.
7 Fleck, N. A., and Newman, J. C., Jr., *Mechanics of Fatigue Crack Closure, ASTM STP 982*, J. C. Newman, Jr. and W. Elber, Eds., ASTM, Philadelphia, PA, 1988, pp. 319-341.
8 Newman, J. C., Jr., *Int J of Fracture*, Vol. 80, 1996, pp. 193-218.
9 Larsen, J. M. and Nicholas, T., *Eng Fracture Mechanics*, Vol. 22, No. 4, 1985, pp. 713-730.
10 Mom, A. J. A, Evans, W. J., and ten Have, A. A., *AGARD Conference Proceedings No. 393, Damage Tolerant Concepts for Critical Engine Components*, AGARD, Neuilly sur Seine, France, 1985, pp. 20-1 - 20-11.
11 Raizenne, M. D., *AGARD Engine Disc Cooperative Test Programme, AGARD Report 766 (Addendum)*, AGARD, Neuilly sur Seine, France, 1993, pp. 4-1 - 4-33.
12 Jany, E. and Renne, O., *AGARD Engine Disc Cooperative Test Programme, AGARD Report 766 (Addendum)*, AGARD, Neuilly sur Seine, France, 1993, pp. 6-1 - 6-83.
13 Topper, T. H. and Yu, M. T., *Int J of Fatigue*, Vol. 7, No. 3, 1985, pp. 159-164.
14 Yu, M. T., Hopper, T. H., and Au, P., *Fatigue 84*, C. J. Beevers, Ed., Engineering Materials Advisory Services Ltd., United Kingdom, Vol. I, 1984, pp. 179-189.
15 Zaiken, E. and Ritchie, R. O., *Engr Fracture Mechanics*, Vol. 22, No. 1, 1985, pp. 35-48.
16 Kardomateas, G. A. and Carlson, R. L., *J of App Mechanics*, Vol. 62, No. 1, 1995, pp. 240-243.
17 Kardomateas, G. A. and Carlson, R. L., *Int J of Fracture*, Vol. 70, No. 2, 1995, pp. 99-115.
18 McClung, R. C. and Sehitoglu, H., *Mechanics of Fatigue Crack Closure, ASTM STP 982*, J. C. Newman, Jr. and W. Elber, Eds., ASTM, Philadelphia, 1988, pp. 279-299.
19 Yang, R., *Int J of Fatigue*, Vol 19, 1994, p.397-402.
20 Sehitoglu, H., Gall, K., and Garcia, A. M., *Int J of Fracture*, Vol. 80, 1996, pp. 165-192.
21 Sun, W. and Sehitoglu, H., *Fatigue and Fracture of Eng Matls and Str*, Vol. 15, No. 2, 1992, pp. 115-128.
22 Sehitoglu, H. and Sun, W., *J of Eng Materials and Tech*, Vol. 113, January 1991, pp. 31-40.
23 Moshier, M.A., Nicholas,T., and Hillberry, B.M., *Int J of Fatigue*, submitted Oct 2000.
24 Lang, M., *Fatigue and Fracture of Eng Matls and Str*, Vol. 23, 2000, pp. 587-601.
25 Lang, M., *Fatigue and Fracture of Eng Matls and Str*, Vol. 23, 2000, pp. 603-617.
26 Redden, T. K., *Beta Titanium Alloys in the 80's*, R. R. Boyer and H. W. Rosenberg, Eds., The Metallurgical Society of AIME, Warrendale, PA, 1984, pp 239-253.
27 E399-90, *Annual Book of ASTM Standards*, American Society of Testing and Materials, Philadelphia, PA, Vol. 03.01, 1999, pp. 422-431.
28 E647-95a, *Annual Book of ASTM Standards*, American Society of Testing and Materials, Philadelphia, PA, Vol. 03.01, 1999, pp. 577-602.
29 Hartman, G. A. and Johnson, D. A., *Experimental Mechanics*, March 1987, pp. 175-229.
30 Larsen, J. M., Worth, B. D., Annis, C. G., Jr., and Haake, F. K., *Int J of Fracture*, Vol. 80, 1996, pp. 237-255.
31 Fleck, N. A., *Acta Metallurgica*, Vol. 33, 1985, pp. 1339-1354.

Paper 21: Discussion

Question from H Pfoertner – MTU, Germany

Do you think that your load interaction method can be generalised to arbitrary load sequences as they occur during real engine operation?

Presenter's Reply

The simple method used for demonstration purposes in this paper would require substantial data generation - testing under all envisioned load interaction scenarios to create the desired multiplication factors - and thus, is probably not suited from the arbitrary case. It was created to quickly emulate, for this specific case, the more general approach of using a K_{pr}-type methodology. This latter approach, I believe, can be generalized for arbitrary load sequences. We are working toward that goal in this and other load-interaction research efforts at the Air Force Research Laboratory. Currently the other co-authors and I are evaluating the appropriateness of K_{pr} for periodic overloads and simple mission spectra as well as periodic underloads. We are striving to better understand the physics of the problem so more general models can be developed with broader applicability.

Question from Dr M Winstone – DSTL, UK

The recovery of K_{pr} was presented in terms of cycles; for Ti alloys, deformation is also time dependent. Would you expect to see a frequency/ramp rate effect? Were the tests done at ramp rates consistent with compressor acceleration and deceleration?

Presenter's Reply

Actually I believe the recovery may be dependent upon the extent of crack propagation for this simple case of periodic underloads. I am presently performing finite element simulations to evaluate the effect of the underload on the stresses/strains/displacements ahead of and behind the crack tip. Immediately after the underload, the simulation suggests some drastic increases in strains a small distance ahead of the crack tip. The recovery may require the crack to grow through this affected region until the steady-state conditions are re-established. Obviously, the accuracy and relevance of this approach is dependent upon the ability to predict the materials constitutive behaviour. Regarding expectations of a frequency effect, the tests were run at nominally 15 Hz, which is much faster than ramp rates experienced under compressor acceleration/deceleration. Interestingly, I have compared my baseline crack growth results (40 Hz) with crack growth rates reported in the AGARD #766 Addendum from 1993 (0.25 Hz). Comparing the two data sets, no frequency effect was noted for Ti-17 from the range of 0.25 to 40 Hz.